Braz J Phys (2016) 46:213–219
DOI 10.1007/s13538-016-0405-8

SOCIEDADE BRASILEIRA DE FÍSICA

CONDENSED MATTER

Electronic and Mechanical Properties of Tetragonal Nb_2Al Under High Pressure: First-Principles Calculations

Zhen Jiao [1,2] · Qi-Jun Liu [1,2] · Fu-Sheng Liu [1,2] · Wen-Peng Wang [1,2] · Yi-Gao Wang [1,2] · Yong Li [1,2] · Zheng-Tang Liu [3]

Received: 1 November 2015 / Published online: 18 February 2016

Abstract We have investigated the structure, density of states, mechanical stability, elastic properties, and Debye temperature of tetragonal Nb_2Al under high pressure using the generalized gradient approximation WC (GGA-WC) functional within density functional theory (DFT). Our obtained lattice constants were in good agreement with the reported experimental and theoretical data at zero pressure. The volume decreased with the increasing pressure. The effects of pressure on the electronic properties have been discussed. The elastic constants under pressure have been calculated, which all satisfied the stability criterion, meaning that tetragonal Nb_2Al was mechanical stability from 0 to 100 GPa. Then, the mechanical properties including bulk modulus B, shear modulus G, Young's modulus E, G/B, and Poisson's ratio ν under pressure were determined using the Voigt-Reuss-Hill method. The G/B value suggested that tetragonal Nb_2Al exhibited ductile behavior under pressure. Poisson's ratio indicated that the interatomic forces in tetragonal Nb_2Al were mainly central forces. Finally, the transverse, longitudinal, and average sound velocities and Debye temperature of tetragonal Nb_2Al under pressure have been estimated.

Keywords Density functional theory · High pressure · Density of states · Elastic properties

1 Introduction

Nb-Al intermetallics have many excellent features such as high melting point, low density, good creep resistance, and good high temperature strength [1–3]. The current researches of Nb-Al intermetallics mainly include Nb_3Al, Nb_2Al, and $NbAl_3$ [4]. Among them, tetragonal Nb_2Al attracts our attention due to its low density, high melting temperature, and high hardness [5]. Moreover, its brittle-ductile transition temperature (BDTT) is higher than 1150 °C and its yield strength is higher than that of monolithic Nb_3Al [6–8].

Within the best of our knowledge, Nb_2Al has been extensively studied experimentally [9–12]. Rios et al. [10] used a Bridgman type facility to directionally solidify Al-Nb eutectic alloy. They found that Nb_2Al grown preferably along the (210) and (420) directions. Leyarovski et al. [11] investigated the superconductivity and magnetic properties of Nb-Al phases. They showed that the superconducting transition temperature and magnetic susceptibility of Nb_2Al were 0.74°K and $(1.0 \pm 0.1) \times 10^{-6}$ emu/g, respectively. Brown et al. [12] investigated the resistivity and lattice parameter variations in Nb_2Al, showing that the electrical resistance of Nb_2Al decreased with the decrease of temperature. Recently, Papadimitriou et al. [13] calculated the lattice constants and elastic constants of Nb_2Al. They obtained the temperature dependence of enthalpy of formation for Nb_2Al. However, the influences of pressure on the structural,

✉ Qi-Jun Liu
qijunliu@home.swjtu.edu.cn

[1] School of Physical Science and Technology, Key Laboratory of Advanced Technologies of Materials, Ministry of Education of China, Southwest Jiaotong University, Chengdu 610031, People's Republic of China

[2] Bond and Band Engineering Group, Sichuan Provincial Key Laboratory (for Universities) of High Pressure Science and Technology, Southwest Jiaotong University, Chengdu 610031, People's Republic of China

[3] State Key Laboratory of Solidification Processing, Northwestern Polytechnical University, Xi'an 710072, People's Republic of China

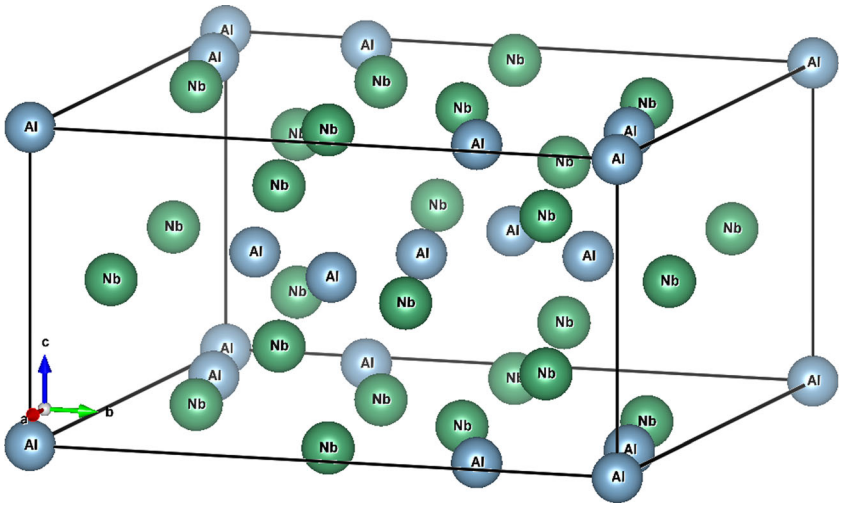

Fig. 1 Crystal structure of tetragonal Nb_2Al [17]

electronic, and mechanical properties have not been studied. Hence, the structural, electronic, elastic, and mechanical properties of tetragonal Nb_2Al were calculated under pressure using the first-principles calculations.

2 Computational Methods

We used the first-principles method based on density functional theory [14] implemented in the CASTEP code [15]. The generalized gradient approximation (GGA) with the WC functional [16] was used as the exchange-correlation function. The energy cutoff for plane-wave was set to be 400 eV. The tolerances of geometry optimization were set as follows: the energy convergence tolerance within 5.0×10^{-6} eV/atom, the maximum force within 0.01 eV/Å, the maximum stress within 0.02 GPa, and the maximum displacement within 5.0×10^{-4} Å. The pseudoatomic calculations were performed for Al $3s^2 3p^1$ and Nb $4s^2 4p^6 4d^4 5s^1$.

3 Results and Discussion

3.1 Crystal Structure Under Pressure

Figure 1 shows the crystal structure of tetragonal Nb_2Al [17], whose space group and Schoenflies notation are $P4_2/mnm$ and D_{4h}^{14} [9]. The calculated lattice constants at zero pressure are listed in Table 1 along with the previous experimental [9–12] and theoretical data [13]. It is noted that our calculated data agree well with the experimental data, indicating that the results are credible. Figure 2 shows the relationship between normalized volume V/V_0 and pressure, where V_0 is our calculated equilibrium volume at zero pressure. It can be seen that the volume decreases with the increasing pressure and the curve is smooth.

3.2 Density of States Under Pressure

Figure 3 shows the total density of states (TDOS) and partial density of states (PDOS) of tetragonal Nb_2Al under zero pressure. The dotted line represents the Fermi level [18], and the resonance in density of states means a sign of the bonding [19]. Then, we can analyze the bonding characteristics in this compound by using the density of states. It is noted that tetragonal Nb_2Al is a conductor from the TDOS of Nb_2Al due to the fact that the TDOS do not have energy gap at Fermi level. The covalent character between Nb and Al atoms appears mainly through the hybridization between Nb-4d and Al-3p states due to the resonance effect near Fermi level. Peaks A and B are located at −54.3 and −30.5 eV. It is found that the Nb-4s and Nb-4p states mainly contribute to peak A and peak B, respectively, which are all isolated states. The size of the pseudogap is related to the

Table 1 Calculated lattice constants of tetragonal Nb_2Al at zero pressure, along with the previous experimental [9–12] and theoretical data [13]

	Lattice constants (Å)	
	a	*c*
This work	9.9083	5.1744
Expt. [9]	9.943	5.186
Expt. [10]	9.9525–9.898	5.169–5.187
Expt. [11]	9.945	5.174
Expt. [12]	9.957–9.914	5.116–5.180
Theor. [13]	9.945	5.119

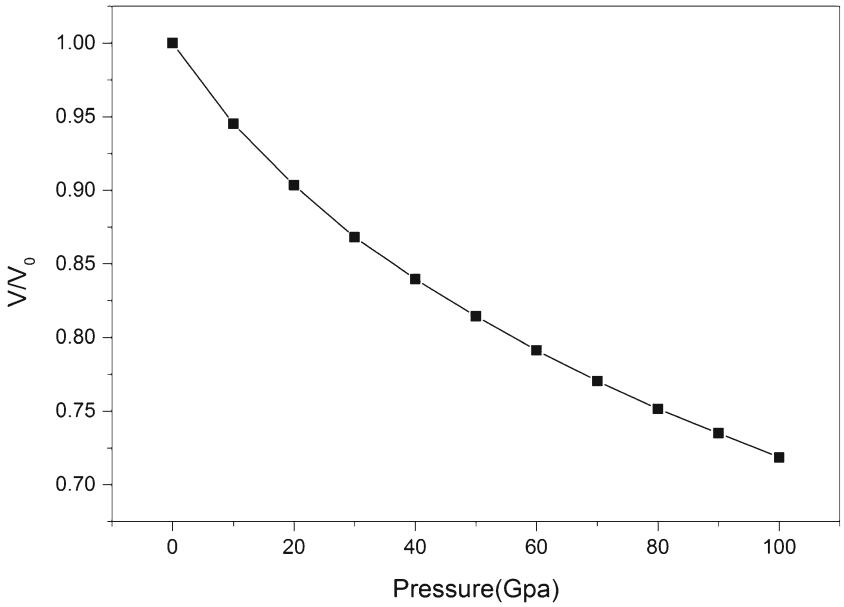

Fig. 2 The relationship between normalized volume V/V_0 and pressure for tetragonal Nb_2Al

strength of covalence [20]. Figure 3 shows a pseudogap existing in the right side of Fermi level, which is located at 1.25 eV.

Figure 4 shows the TDOS of Nb_2Al under 0, 50, and 100 GPa. The shape of TDOS curves suggests that the structure of Nb_2Al keeps stable when the pressure increases up to 100 GPa. The TDOS near Fermi level have been broadened with the pressure increasing to 100 GPa. The TDOS range from −8.8 to 10.9 eV at zero pressure, from −9.5 to 13.1 eV at 50 GPa, and from −10.1 to 14.2 eV at 100 GPa, indicating that the hybridization between Nb-4d and Al-3p states is enhanced with the increasing pressure. How about the stability of other Al-based compounds under pressure? Zhang and Jiang demonstrated that Al_3Er and Al_3Yb were stable up to 100 GPa [21]. Hou et al. [22] calculated the structural, elastic, thermodynamic, and electronic properties of $L1_2$-ordered Ni_3Al, showing that it was mechanically stable and had no structural phase transition up to 50 GPa. Liu et al. [23] studied the phase transition and electronic structure of Pt_3Al alloys, showing that there was a phase transition from tetragonal phase to cubic phase at 60 GPa and the hybridization between Pt and Al atoms were enhanced under pressure.

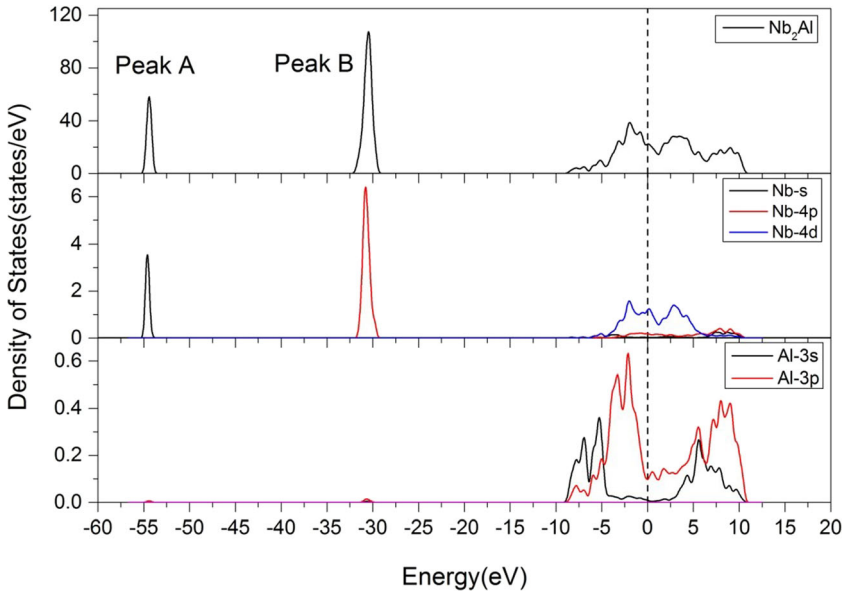

Fig. 3 TDOS and PDOS of Nb_2Al under zero pressure

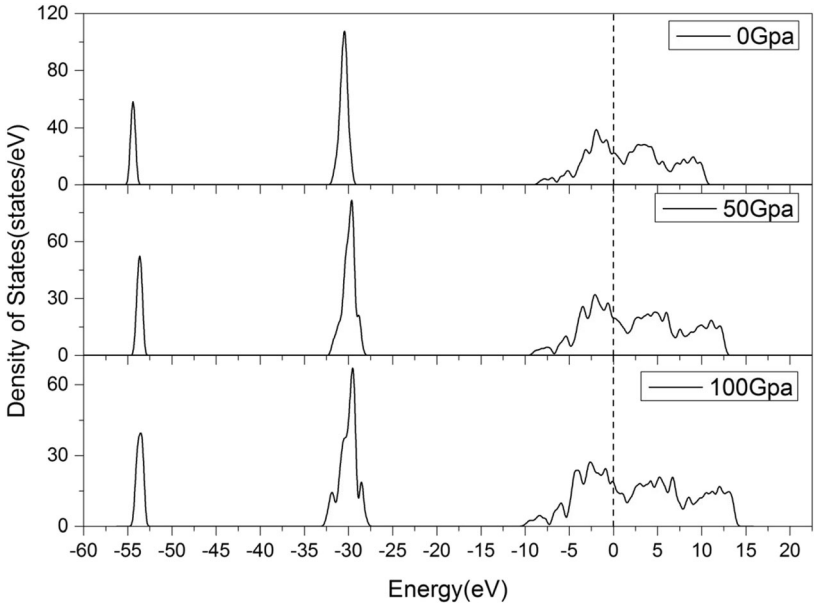

Fig. 4 TDOS of Nb_2Al under 0, 50, and 100 GPa

3.3 Mechanical Properties Under Pressure

Elastic constants are important information for materials. For tetragonal crystal system, the elastic coefficient matrix has six independent nonzero elastic stiffness constants, including C_{11}, C_{12}, C_{13}, C_{33}, C_{44}, and C_{66}. The calculated elastic constants at zero pressure are $C_{11} = 273.2$ GPa, $C_{12} = 112.9$ GPa, $C_{13} = 87.2$ GPa, $C_{33} = 324.1$ GPa, $C_{44} = 69.6$ GPa, and $C_{66} = 82.4$ GPa, which are in agreement with previous theoretical data [13]. The elastic constants of tetragonal Nb_2Al under pressure are shown in Fig. 5. The elastic constants C_{11}, C_{12}, C_{13}, C_{33}, and C_{44} increase with the increasing pressure up to 100 GPa, but there is a decrease for C_{66} at 40 GPa.

If the elastic constants satisfy the Born stability criterion [24–26] (the criterion for a stable crystal requires a positive determinant for the crystal's symmetric matrix), the crystal structure is mechanically stable. The stability criterion is as follows:

$$\begin{aligned}&(C_{11}-P) > 0,\ (C_{33}-P) > 0,\ (C_{44}-P) > 0,\ (C_{66}-P) > 0,\\ &(C_{11}-C_{12}-2P) > 0, (C_{11}+C_{33}-2C_{13}-4P) > 0,\\ &(2C_{11}+2C_{12}+C_{33}+4C_{13}+3P) > 0\end{aligned} \quad (1)$$

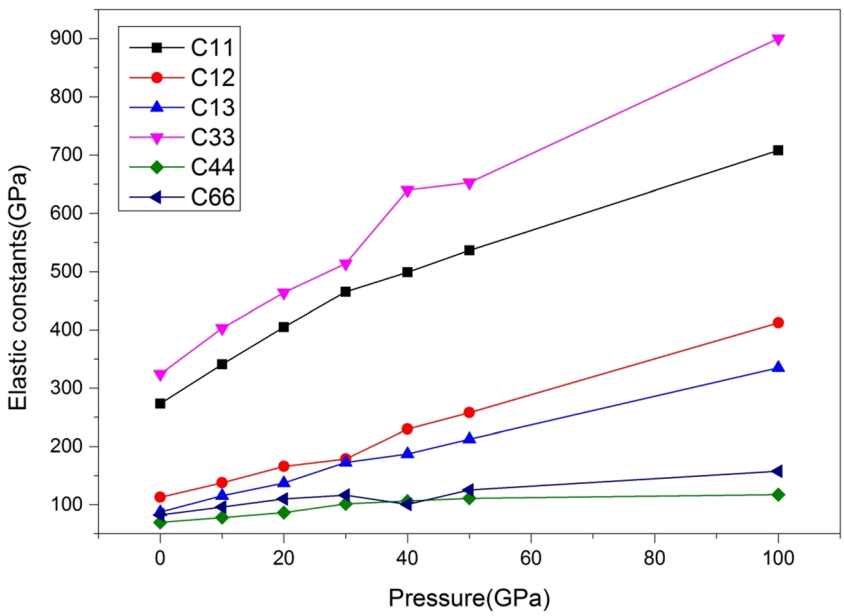

Fig. 5 Pressure dependence of elastic constants of tetragonal Nb_2Al

Table 2 Calculated bulk modulus, shear modulus, Young's modulus, Poisson's ratio, and G/B at zero pressure along with previous theoretical data [13]

	B (GPa)	G (GPa)	E (GPa)	ν	G/B
This work	160.5	81.8	209.8	0.282	0.510
Theor. [13]	161.5	72.3	188.7	0.305	0.448

It is suggested that tetragonal Nb_2Al is mechanically stable from 0 to 100 GPa.

The E, B, and G represent Young's modulus, bulk modulus, and shear modulus [27, 28], respectively, which are obtained by using the Voigt-Reuss-Hill approximation [29–33]. The bulk and shear modulus related to Voigt and Reuss approximations can be obtained as follows [32]:

$$\begin{aligned} B_V &= \frac{2(C_{11}+C_{12})+C_{33}+4C_{13}}{9} \\ G_V &= \frac{(M+3C_{11}-3C_{12}+12C_{44}+6C_{66})}{30} \\ B_R &= \frac{C^2}{M} \\ G_R &= 15\left(\frac{18B_V}{C^2}+\frac{6}{C_{11}-C_{12}}+\frac{6}{C_{44}}+\frac{3}{C_{66}}\right)^{-1} \\ M &= C_{11}+C_{12}+2C_{33}-4C_{13} \\ C^2 &= (C_{11}+C_{12})C_{33}-2C^2_{13} \end{aligned} \quad (2)$$

The Hill approximation is an average value from the Voigt and Reuss approximations. Then, Young's modulus and Poisson's ratio of Nb_2Al are calculated:

$$\frac{1}{E}=\frac{1}{3G}+\frac{1}{9B} \quad (3)$$

$$\nu=\frac{1}{2}\left[1-\frac{3G}{3B+G}\right] \quad (4)$$

Calculated bulk modulus, shear modulus, Young's modulus, Poisson's ratio, and G/B at zero pressure are listed in Table 2 along with previous theoretical data [13]. The obtained mechanical properties agree well with the theoretical data [13], indicating that the GGA-WC functional can well describe the stress-strain relationship. Figure 6 shows the pressure dependence of Young's modulus, shear modulus, and bulk modulus. It is noted that Young's modulus, shear modulus, and bulk modulus monotonically increase with the pressure increasing up to 100 GPa.

Figure 7 shows the calculated ratio of shear modulus to bulk modulus (G/B), the universal anisotropy index, and the Poisson's ratio as functions of pressure. The ratio of shear modulus to bulk modulus (G/B) can roughly estimate the ductile/brittle property of materials [34]. It is well known that shear modulus G represents the resistance to plastic deformation and bulk modulus B represents the resistance to fracture. A low G/B ratio corresponds to the ductile nature, and a high value associates with the brittle behavior due to the fact that the relatively easy/difficult plastic flow induces low/high stress concentration at the root of a crack. The threshold is 0.57; that is, the material behaves in a brittle form when G/B > 0.57. Otherwise, the material exhibits a ductile behavior. In Fig. 7, it is seen that the G/B values from 0 to 100 GPa are all smaller than 0.57, suggesting that tetragonal Nb_2Al exhibits ductile behavior under pressure up to 100 GPa. Moreover, the ductile property is increased with the increasing pressure.

Poisson's ratio is a reflection of lateral deformation of the elastic constants for materials, which can be used to

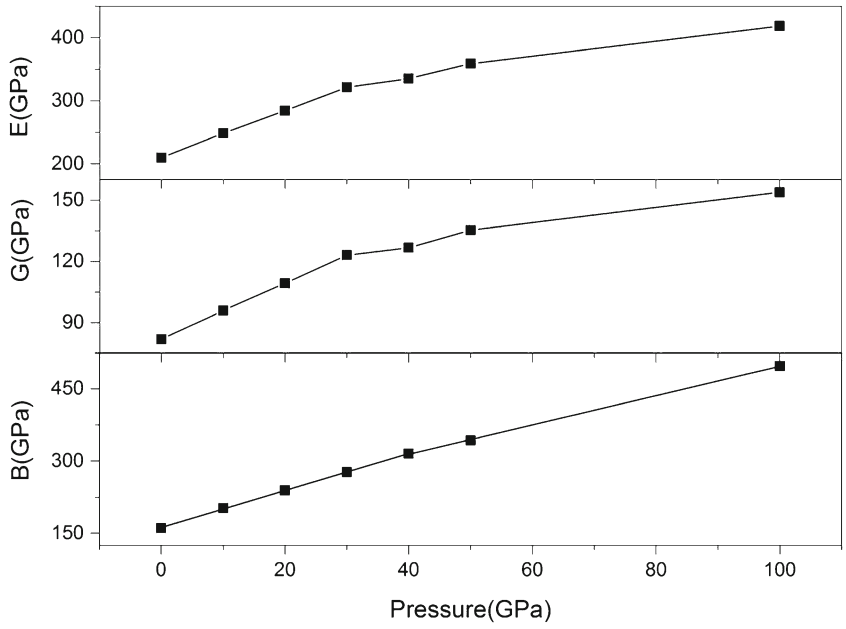

Fig. 6 Pressure dependence of Young's modulus, shear modulus, and bulk modulus

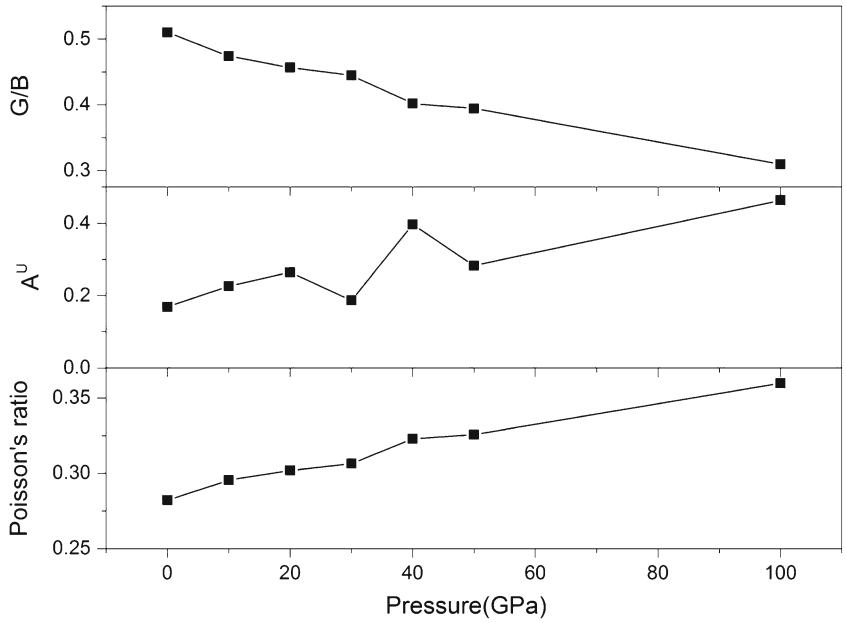

Fig. 7 Calculated ratio of shear modulus to bulk modulus, the universal anisotropy index, and the Poisson's ratio as functions of pressure

quantify the stability against shear deformation [35, 36]. Moreover, the better plasticity of materials is associated with the larger Poisson's ratio [37]. In Fig. 7, Poisson's ratio increases with the increase of pressure, showing that the plasticity of Nb_2Al increases with the increasing pressure. Poisson's ratio gives a lot of information about the characteristics of the bonding forces, and the upper and lower limits for central force solids are 0.5 and 0.25 [38], respectively. Our calculated Poisson's ratio ranges from 0.28 to 0.36 with the pressure increasing to 100 GPa, meaning that the interatomic forces in Nb_2Al are mainly central forces.

The universal anisotropy index (A^U) can be obtained from the B_{Voigt}, G_{Voigt}, B_{Reuss}, and G_{Reuss} as follows [39]:

$$A^U = 5\frac{G_V}{G_R} + \frac{B_V}{B_R} - 6 \tag{5}$$

A^U describes the degree of anisotropy for crystals [40]. If the universal anisotropy index is zero, the crystal shows isotropy. It is noted that Nb_2Al is anisotropic under pressure, and the degree of anisotropy for Nb_2Al approximately increases with the increase of pressure.

Debye temperature (Θ_D) provides useful information for understanding thermodynamic properties of materials, such as specific heat capacity, thermal expansion coefficient, and melting point [41]. The elastic constants and the wave velocities can estimate the Debye temperature. This method obtaining Debye temperature is the same as that obtained from specific heat measurements at low temperatures [42]. The Debye temperature of Nb_2Al compound is obtained from the average sound velocity (V_m) [43]:

$$\Theta_D = \frac{h}{k_B}\left[\frac{3nN_A\rho}{4\pi M}\right]^{\frac{1}{3}} V_m \tag{6}$$

where h is Planck's constant ($h = 6.626 \times 10^{-34}$ J·S), k_B is Boltzmann's constant ($k_B = 1.381 \times 10^{-23}$ J/K), n is the number of atoms per formula unit ($n(Nb_2Al) = 3$), N_A is Avogadro's number ($N_A = 6.022 \times 10^{23}$/mol), and M is the molecular weight ($M(Nb_2Al) = 212.8$ g/mol).

The average wave velocity (V_m) of polycrystalline materials can be obtained from the transverse (V_t) and longitudinal sound velocities (V_l), which are as follows:

$$V_m = \left[\frac{1}{3}\left(\frac{1}{V_l^3} + \frac{2}{V_t^3}\right)\right]^{-\frac{1}{3}} \tag{7}$$

$$V_t = \sqrt{\frac{G}{\rho}} \tag{8}$$

Table 3 Pressure dependence of density, transverse, longitudinal, and average sound velocities, and Debye temperature of Nb_2Al compound

Pressure (GPa)	ρ (g/cm^3)	V_t (m/s)	V_l (m/s)	V_m (m/s)	Θ_D (K)
0	6.956	3430	6226	3823	443
10	7.359	3611	6700	4031	476
20	7.699	3767	7071	4209	505
30	8.012	3919	7417	4381	532
40	8.283	3911	7647	4381	538
50	8.541	3980	7829	4460	554
100	9.680	3986	8516	4487	581

$$V_l = \sqrt{\frac{B + \frac{4}{3}G}{\rho}} \quad (9)$$

Table 3 shows the pressure dependence of density, transverse, longitudinal, and average sound velocities, and Debye temperature of Nb_2Al compound. Our calculated Debye temperature of Nb_2Al at zero pressure is higher than that reported in [13], which waits for experimental verification. Our calculations show that the Debye temperature and the transverse, longitudinal, and average sound velocities approximately increase with the increasing pressure, indicating that pressure has much influence on Nb_2Al compound.

4 Conclusions

The paper has used the GGA-WC functional to investigate the pressure dependence of structure, density of states, mechanical stability, and elastic properties of Nb_2Al. Our calculated lattice constants were in good agreement with the previous experimental and theoretical data at zero pressure. The DOS showed that Nb_2Al was a conductor. The Nb and Al atoms were bonded mainly through the hybridization between Nb-4d and Al-3p states. The density of states near the Fermi level has been broadened with the increase of pressure. The calculated elastic constants satisfied stability criterion under pressure, indicating that Nb_2Al was mechanically stable from 0 to 100 GPa. The G/B values showed that Nb_2Al exhibited ductile behavior under pressure up to 100 GPa. The universal anisotropic index (A^U) suggested that Nb_2Al was anisotropic under pressure. Poisson's ratio indicated that the interatomic forces of Nb_2Al were central forces. The relationship of Debye temperature and pressure showed that the stress had much influence on Nb_2Al compound.

Acknowledgments This work was supported by the National Natural Science Foundation of China (Grant Nos. 51402244 and 11547311), the Fundamental Research Fund for the Central Universities, China (Grant Nos. 2682014ZT30 and 2682014ZT31), the fund of the State Key Laboratory of Solidification Processing in NWPU (Grant No. SKLSP201511), and the Graduate Innovative Experimental Practice Program of SWJTU (Grant No. YC201511101).

References

1. B.A. Glowacki, Intermetallics **7**, 117–140 (1999)
2. B.A. Glowacki, X.-Y. Yan, D. Fray, G. Chen, M. Majoros, Y. Shi, Physica C **372–376**, 1315–1320 (2002)
3. E.I. Gladyshevskii, Zhurnal Strukturnoi Khimii **2**, 158–161 (1961)
4. N. Wang, C. Du, J.G. Hou, Y. Zhang, K. Huang, S.Q. Jiao, H.M. Zhu, Intermetallics **43**, 45–52 (2013)
5. A.K. Bhattacharya, J. Am. Ceram. Soc. **75**, 1678–1681 (1992)
6. S. Hanada, Curr. Opin. Solid State Mater. Sci. **2**, 279–283 (1997)
7. S. Hanada, T. Tabaru, R. Guanamoorthy, Acta Metall. Sin. **8**, 477–487 (1995)
8. M. Luo, H.M. Chen, H.C. Wang, L.J. He, X. Li, Chin J Nonferrous Metals **21**, 72–79 (2011)
9. C.R. McKinsey, G.M. Faulring, Acta Crystallogr. **12**, 701–702 (1959)
10. C.T. Rios, P.L. Ferrandini, S. Milenkovic, R. Caram, Mater. Charact. **54**, 187–193 (2005)
11. E. Leyarovski, L. Leyarovska, E. Krasnopyorov, L. Kokot, R. Horyń, T. Mydlarz, Z. Physik B **27**, 57–60 (1977)
12. P.W. Brown, F.J. Worzala, J. Mater. Sci. **11**, 760–766 (1976)
13. I. Papadimitriou, C. Utton, P. Tsakiropoulos, Comput. Mater. Sci. **107**, 116–121 (2015)
14. P. Hohenberg, W. Kohn, Phys. Rev. **136**, 864–871 (1964)
15. S.J. Clark, M.D. Segall, C.J. Pickard, P.J. Hasnip, M.I.J. Probert, K. Refson, M.C. Payne, Z. Kristallogr. **220**, 567–570 (2005)
16. Z.G. Wu, R.E. Cohen, Phys. Rev. B **73**, 235116 (2006)
17. K. Momma, F. Izumi, J. Appl. Crystallogr. **44**, 1272 (2011)
18. C.A. Mead, W.G. Spitzer, Phys. Rev. **134**, A713–A716 (1964)
19. N. Saikia, S.K. Pati, R.C. Deka, Appl. Nanosci. **2**, 389–400 (2012)
20. N.F. Mott, Philos. Mag. **19**, 835–852 (1969)
21. X.D. Zhang, W. Jiang, Philos. Mag. doi:10.1080/14786435.2015.1132851.
22. H. Hou, Z.Q. Wen, Y.H. Zhao, L. Fu, N. Wang, P.D. Han, Intermetallics **44**, 110 (2014)
23. Y.J. Liu, H.W. Huang, Y. Pan, G.H. Zhao, Z. Liang, J. Alloys Compd. **597**, 200 (2014)
24. G.V. Sin'ko, N.A. Smirnov, J. Phys. Condens. Matter **14**, 6989 (2002)
25. G.V. Sin'ko, N.A. Smirnov, J. Phys. Condens. Matter **16**, 8101 (2004)
26. Q.J. Liu, Z. Ran, F.S. Liu, Z.T. Liu, J. Alloys Compd. **631**, 192–201 (2015)
27. A. Gueddim, N. Bouarissa, A. Villesuzanne, Comput. Mater. Sci. **48**, 490–494 (2010)
28. X.D. Li, B. Bhushan, Mater Charact **48**, 11–36 (2002)
29. W. Voigt, *Lehrbuch der Kristallphysik* (Teubner, Leipzig, 1928)
30. A. Reuss, Z. Angew. Math. Mech. **9**, 49 (1929)
31. R. Hill, Proc. Phys. Soc. Lond. **65**, 349 (1952)
32. Z.J. Wu, E.J. Zhao, H.P. Xiang, X.F. Hao, X.J. Liu, J. Meng, Phys. Rev. B **76**, 054115 (2007)
33. I. Papadimitriou, C. Utton, P. Tsakiropoulos, Acta Mater. **86**, 23–33 (2015)
34. S.F. Pugh, Philos. Mag. **45**, 823 (1954)
35. B. Mayer, H. Anton, E. Bott, M. Methfessel, J. Sticht, J. Harris, P.C. Schmidt, Intermetallics **11**, 23–32 (2003)
36. G.N. Greaves, A.L. Greer, R.S. Lakes, T. Rouxel, Nat. Mater. **10**, 823–837 (2011)
37. D. Chen, Z. Chen, Y. Wu, M.L. Wang, N.H. Ma, H.W. Wang, Intermetallics **52**, 64–71 (2014)
38. H.Z. Fu, D.H. Li, F. Peng, T. Gao, X.L. Cheng, Comput. Mater. Sci. **44**, 774–778 (2008)
39. S.I. Ranganathan, M. Ostoja-Starzewski, Phys. Rev. Lett. **101**, 055504 (2008)
40. C.Y. Pu, L. Wang, L.X. Lü, R.M. Yu, C.Z. He, Z.W. Lu, D.W. Zhou, Acta Phys. Sin. **64**, 087103 (2015)
41. H.Z. Wang, Y.Z. Zhan, M.J. Pang, Comput. Mater. Sci. **54**, 16–22 (2012)
42. G. Leibfried, W. Ludwig, Solid State Phys. **12**, 275 (1961)
43. O.L. Anderson, J. Phys. Chem. Solids **24**, 909 (1963)